Electronic Supporting Information

Ni(II)-dithiocarbamate and -diphosphine coordination complexes as pre-catalysts for electrochemical OER activity

Sarvesh Kumar Pal[a], Toufik Ansari[b], Chote Lal Yadav[a], Nanhai Singh[a]. Prem Lama[c*], Arindam Indra[b]*, Kamlesh Kumar[a]*

[a] *Department of Chemistry, Institute of Science, Banaras Hindu University, Varanasi-221005, India*

[b]*Department of Chemistry, Indian Institute of Technology, Banaras Hindu University, Varanasi-221005, India*

[c]*CSIR-Indian Institute of Petroleum, Nanocatalysis Area, LSP Division, Mohkampur, Dehradun-248005, India*

Email Address of Corresponding Authors: kamlesh.kumar@bhu.ac.in (Kamlesh Kumar) arindam.chy@iitbhu.ac.in (Arindam Indra), prem.lama@iip.res.in (Prem Lama)

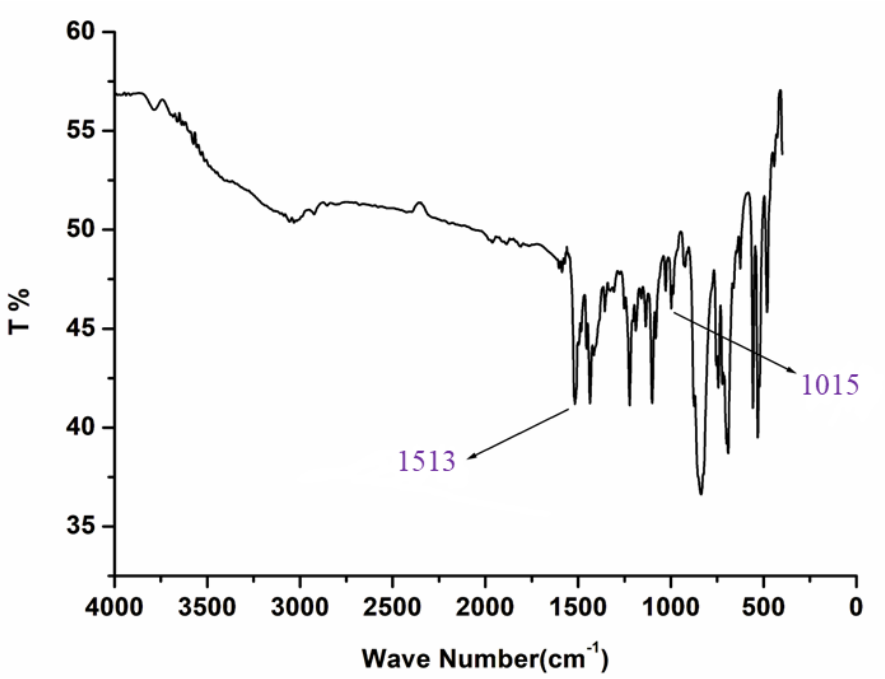

Fig. S1a: FT-IR spectrum of complex **1**.

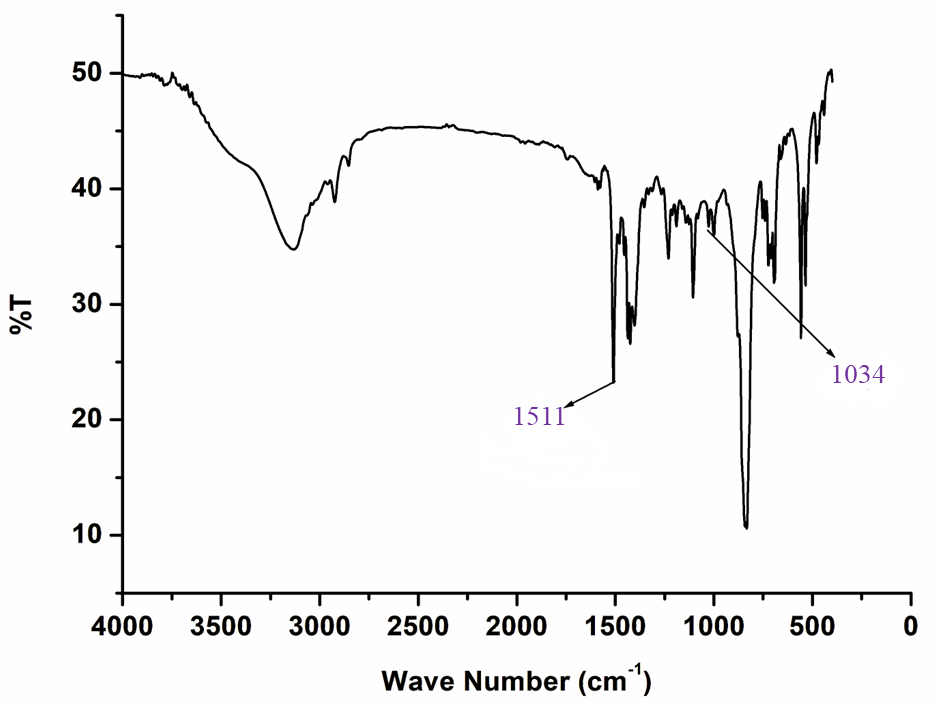

Fig. S1b: FT-IR spectrum of complex **2**.

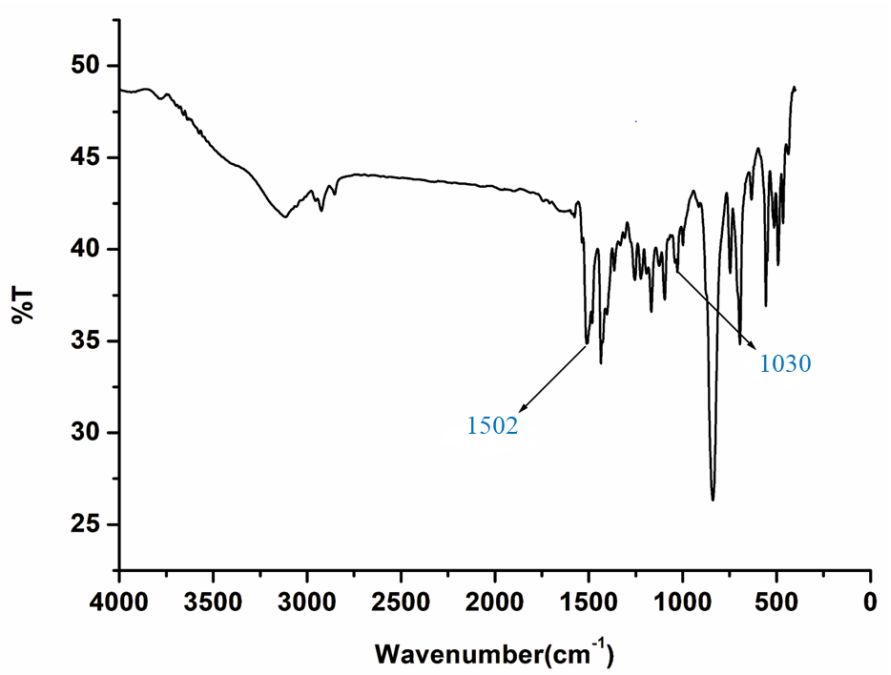

Fig. S1c: FT-IR spectrum of complex **3**.

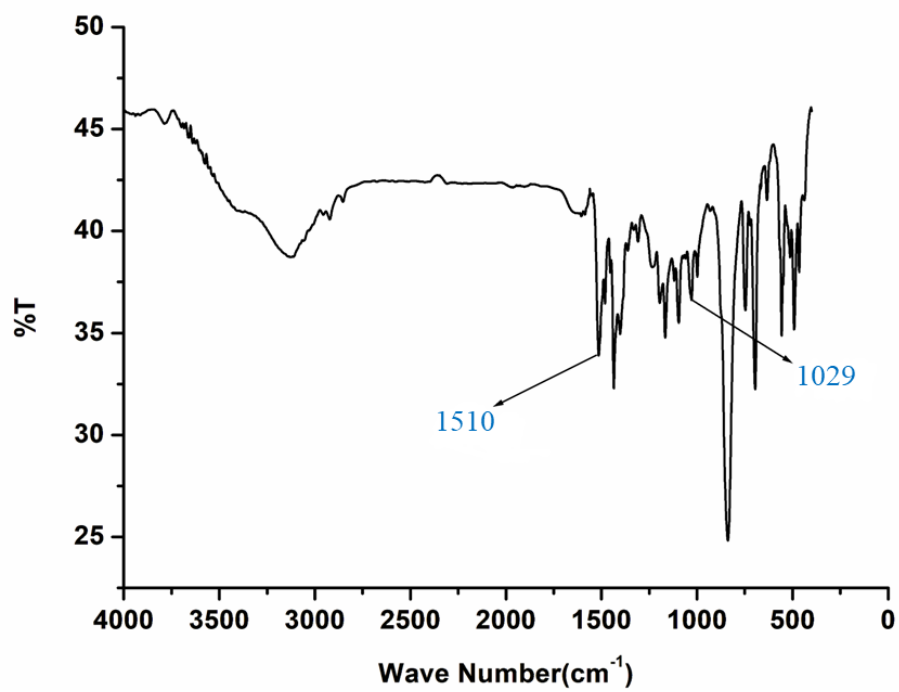

Fig. S1d: FT-IR spectrum of complex **4**.

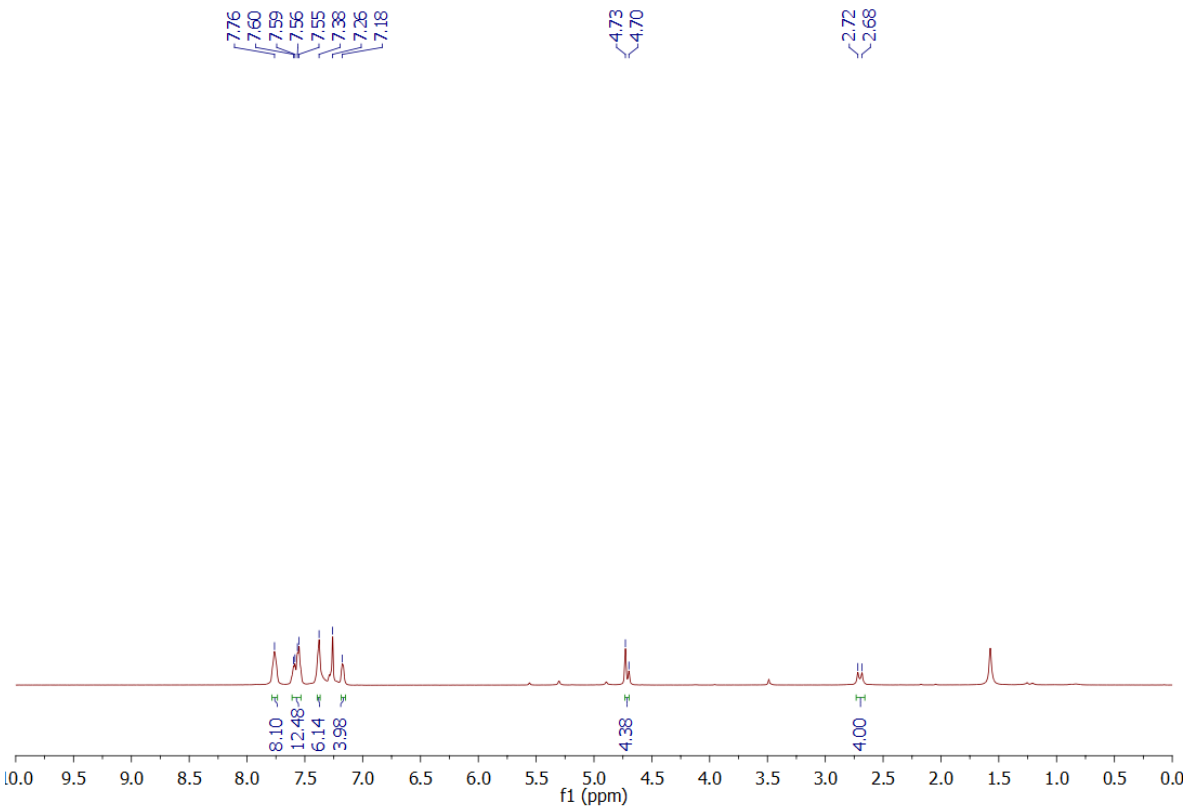

Fig. S2a: ^{1}H NMR spectrum (500 MHz, $CDCl_3$) of complex **1**.

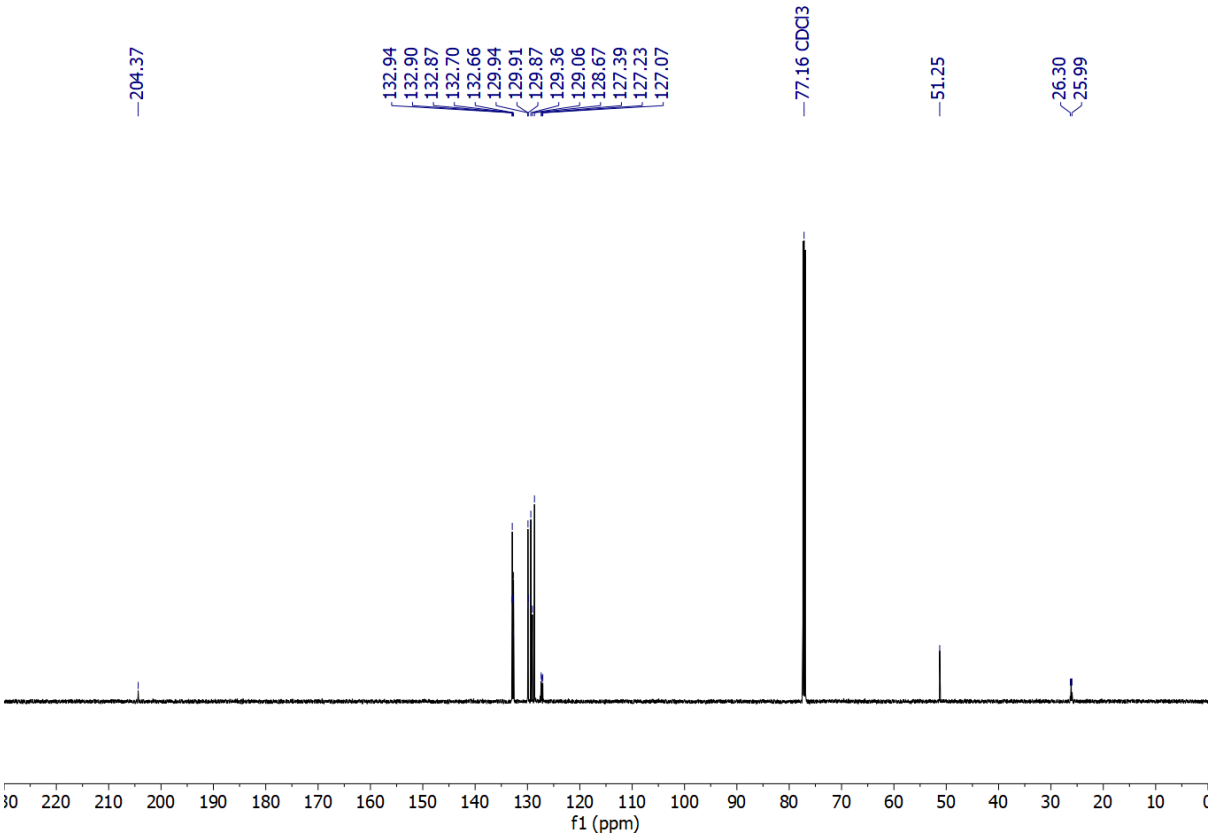

Fig. S2b: $^{13}C\{^{1}H\}$ NMR spectrum (125 MHz, $CDCl_3$) of complex **1**.

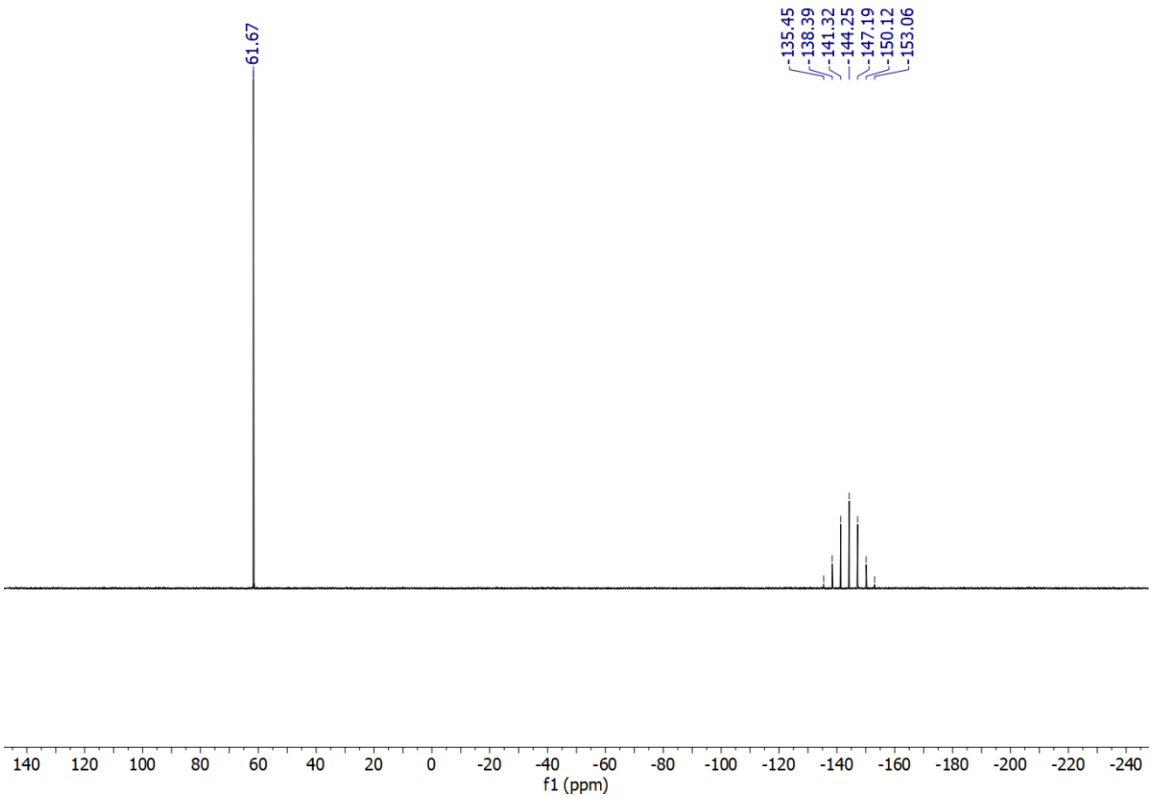

Fig. S2c: $^{31}P\{^{1}H\}$ NMR spectrum (202 MHz, $CDCl_3$) of complex **1**.

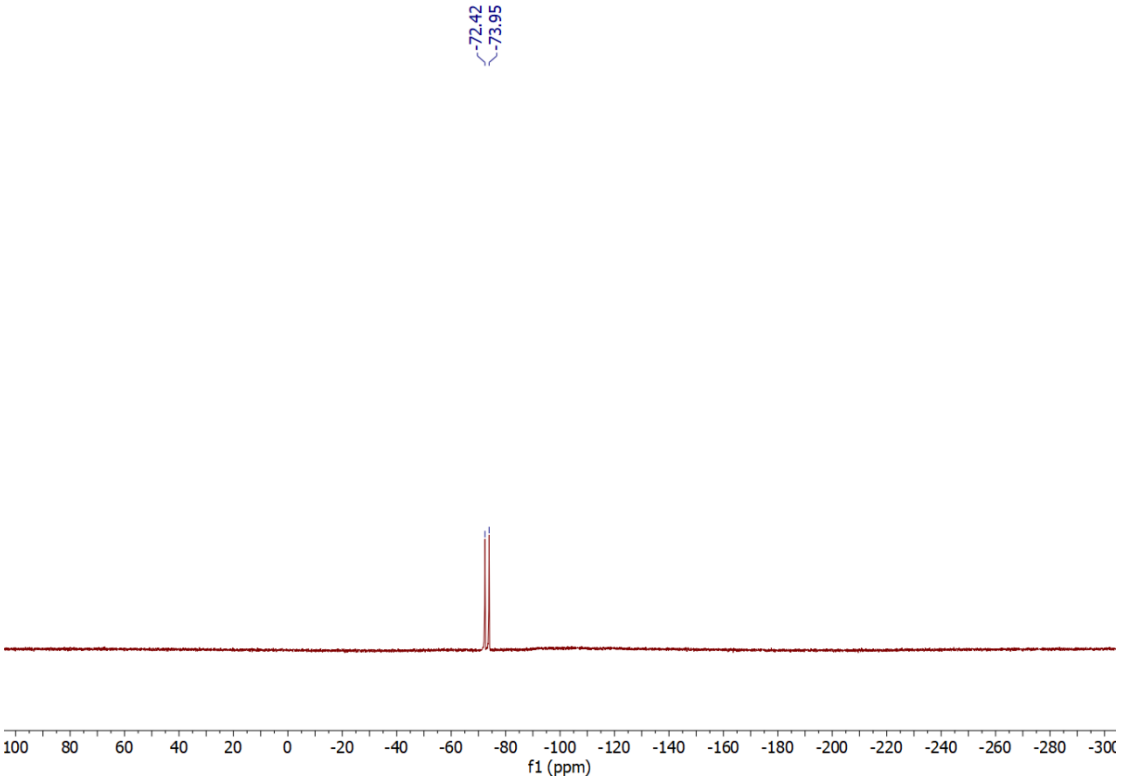

Fig. S2d: $^{19}F\{^{1}H\}$ NMR spectrum (470 MHz, $CDCl_3$) of complex **1**.

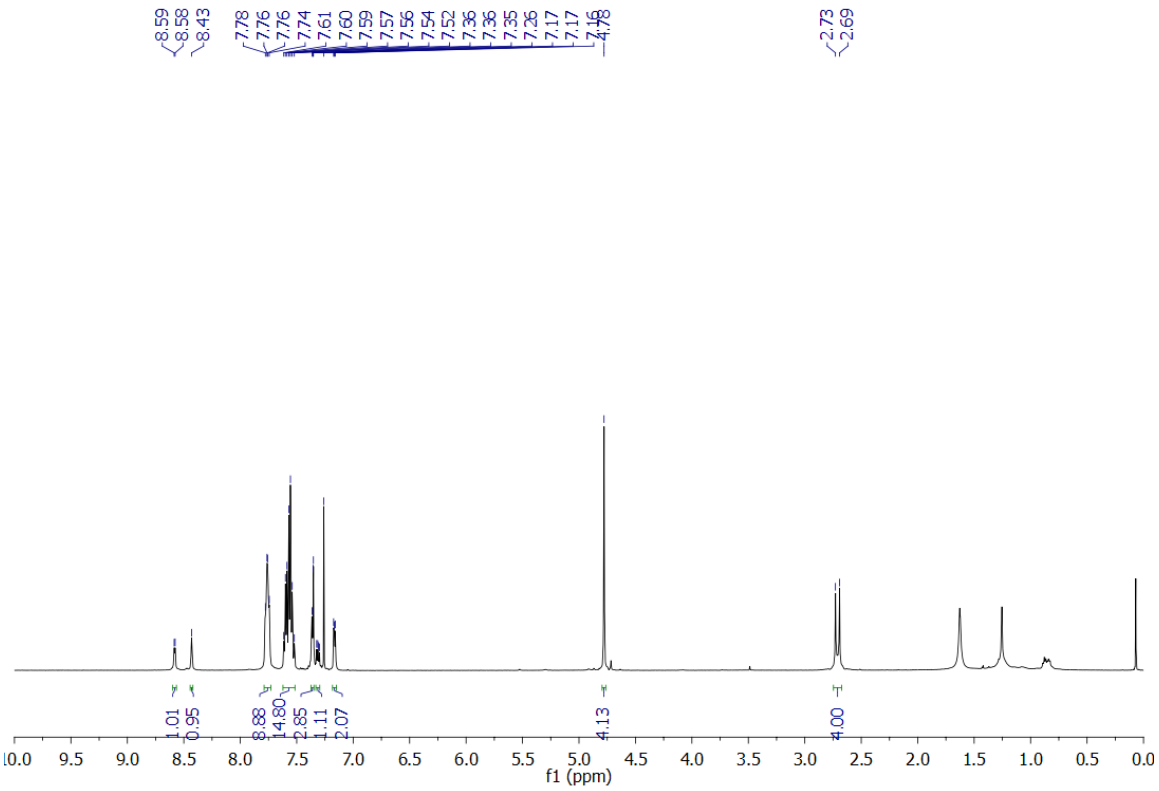

Fig. S2e: ^{1}H NMR spectrum (500 MHz, $CDCl_3$) of complex **2**.

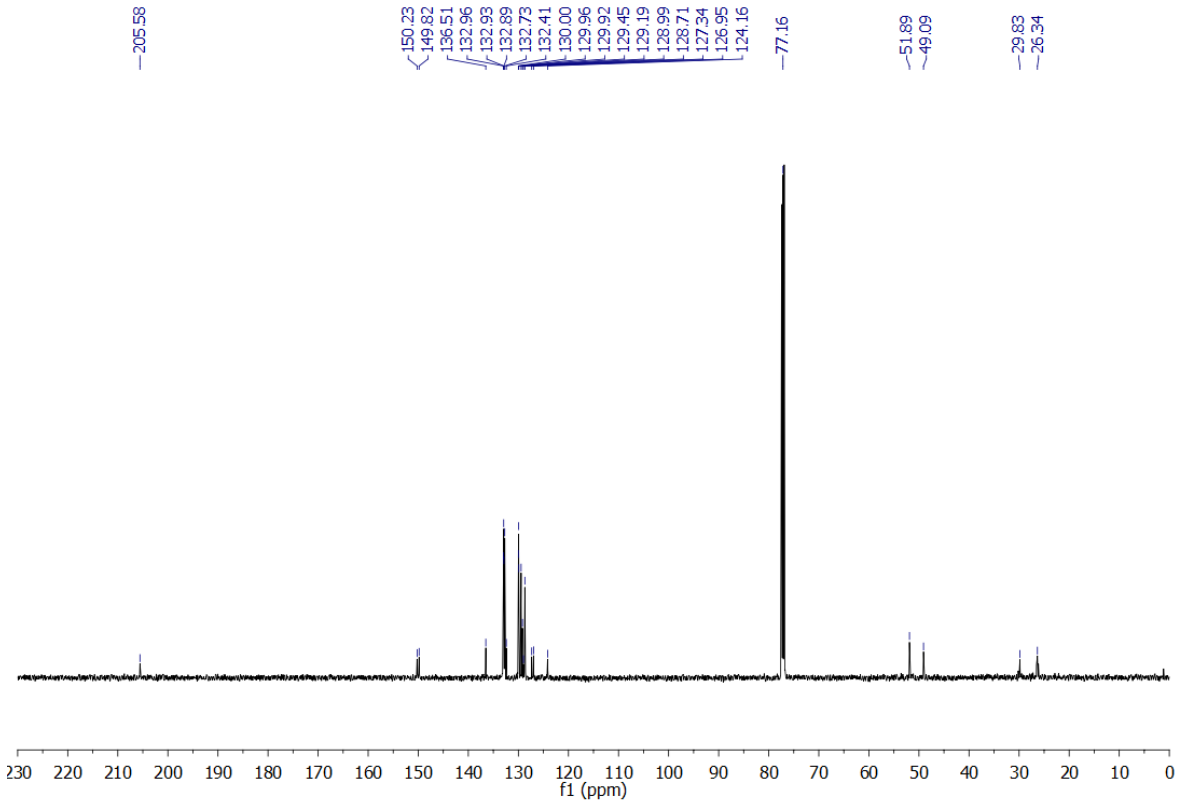

Fig. S2f: $^{13}C\{^{1}H\}$ NMR spectrum (125 MHz, $CDCl_3$) of complex **2**.

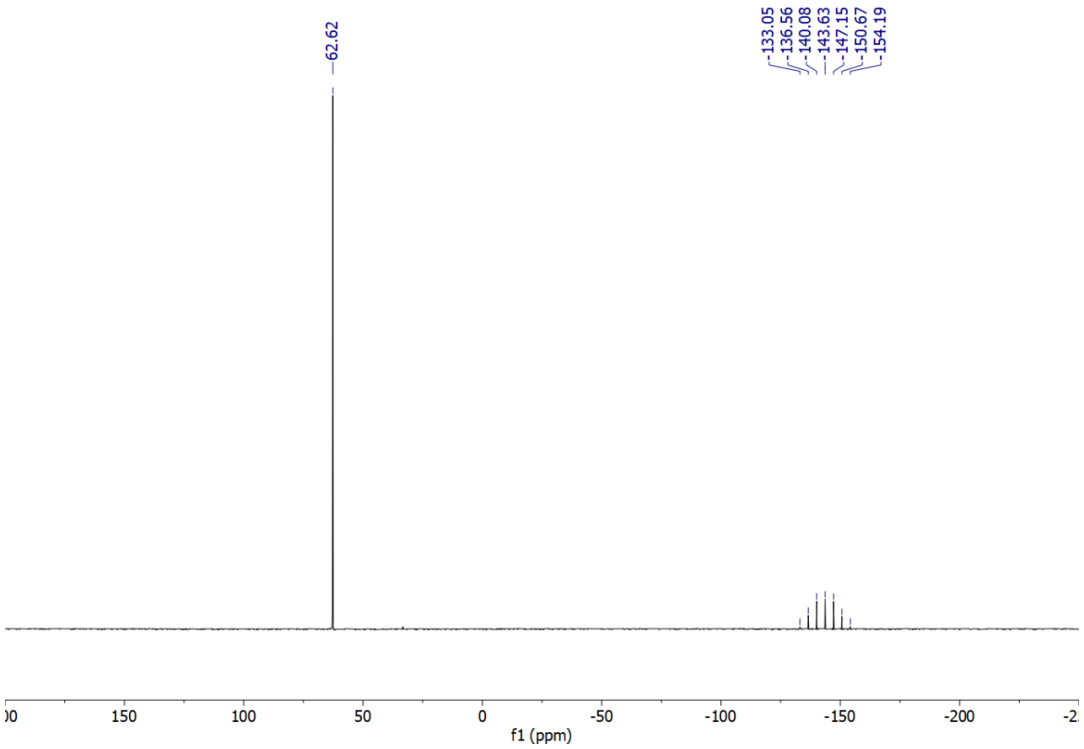

Fig. S2g: $^{31}P\{^{1}H\}$ NMR spectrum (202 MHz, $CDCl_3$) of complex **2**.

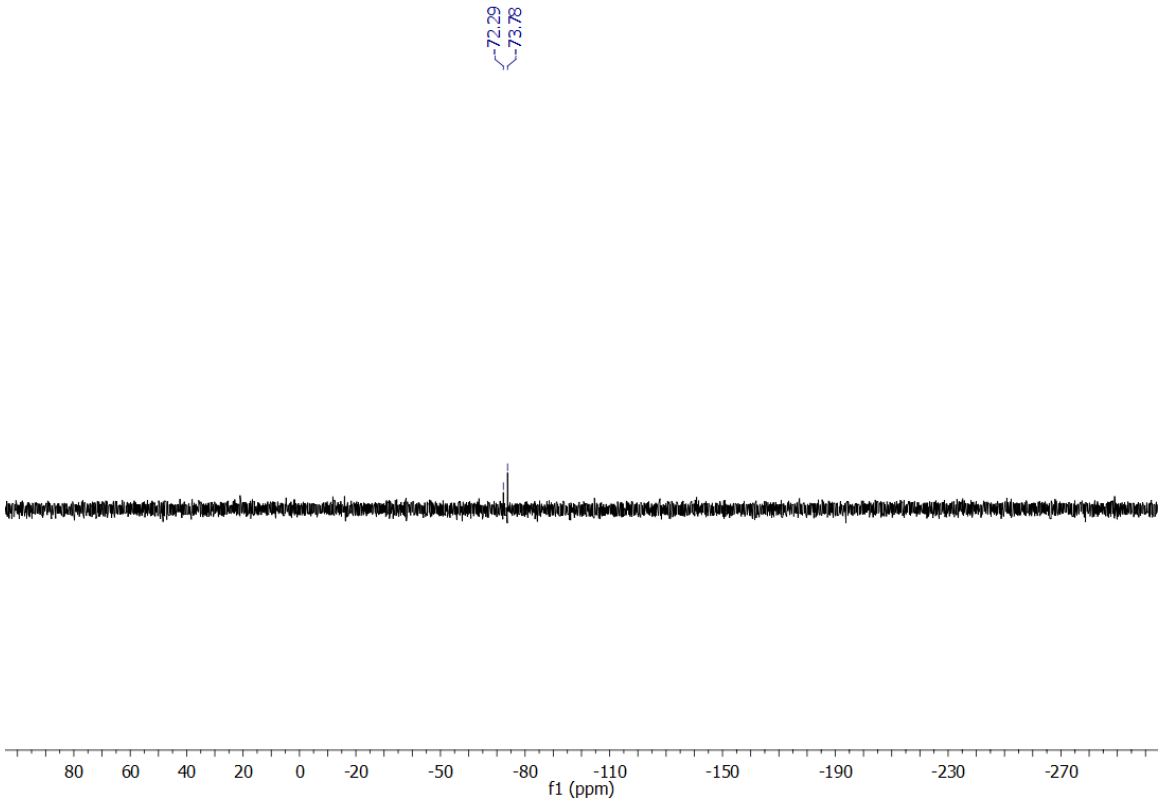

Fig. S2h: $^{19}F\{^{1}H\}$ NMR spectrum (470 MHz, $CDCl_3$) of complex **2**.

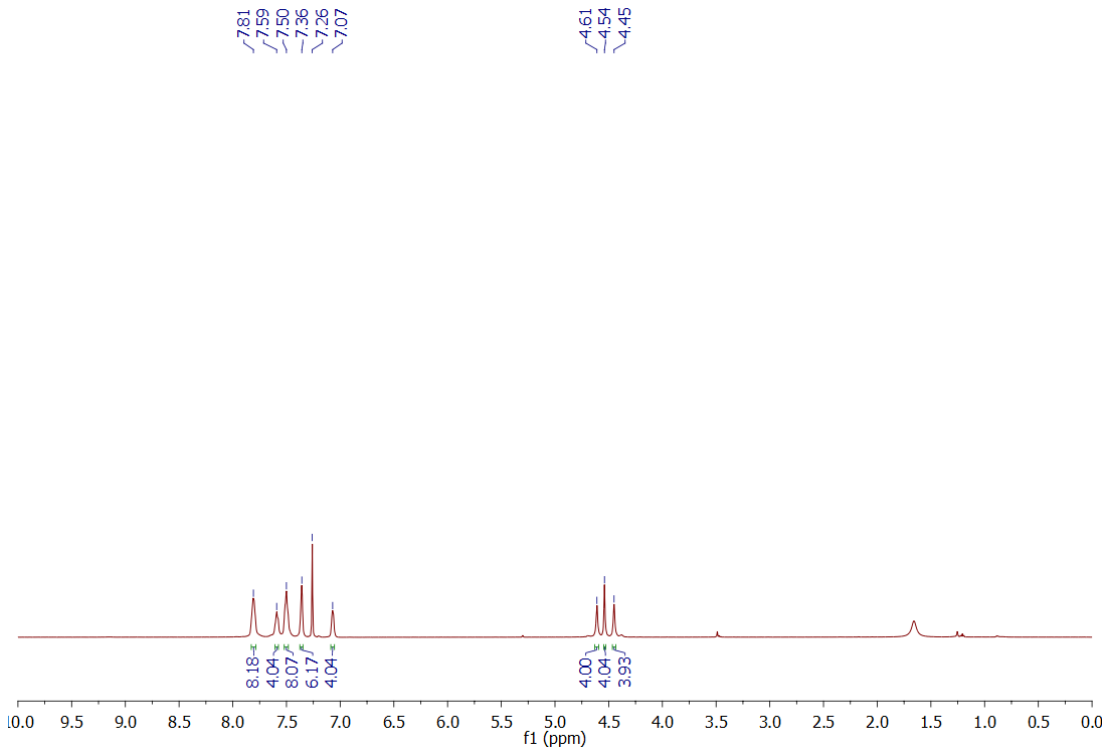

Fig. S2i: ^{1}H NMR spectrum (500 MHz, $CDCl_3$) of complex **3**.

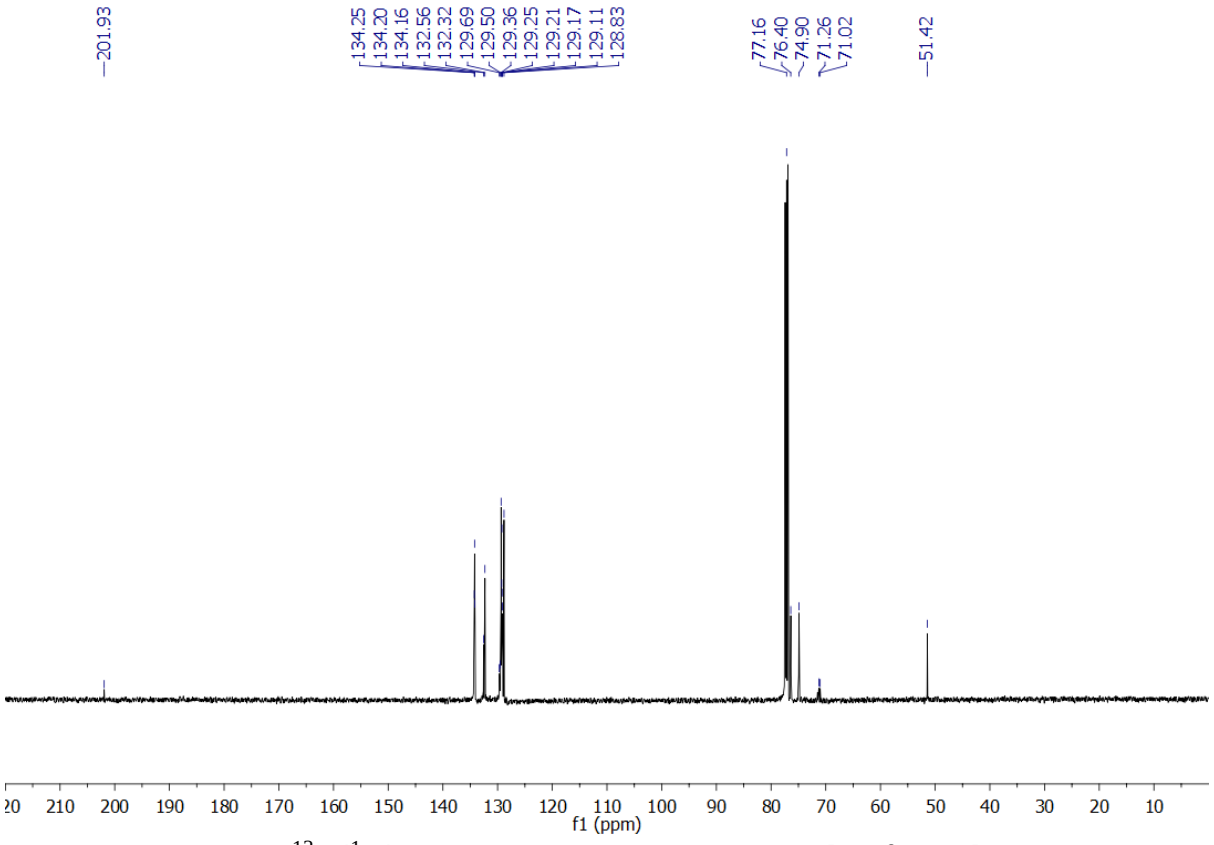

Fig. S2j: $^{13}C\{^{1}H\}$ NMR spectrum (125 MHz, $CDCl_3$) of complex **3**.

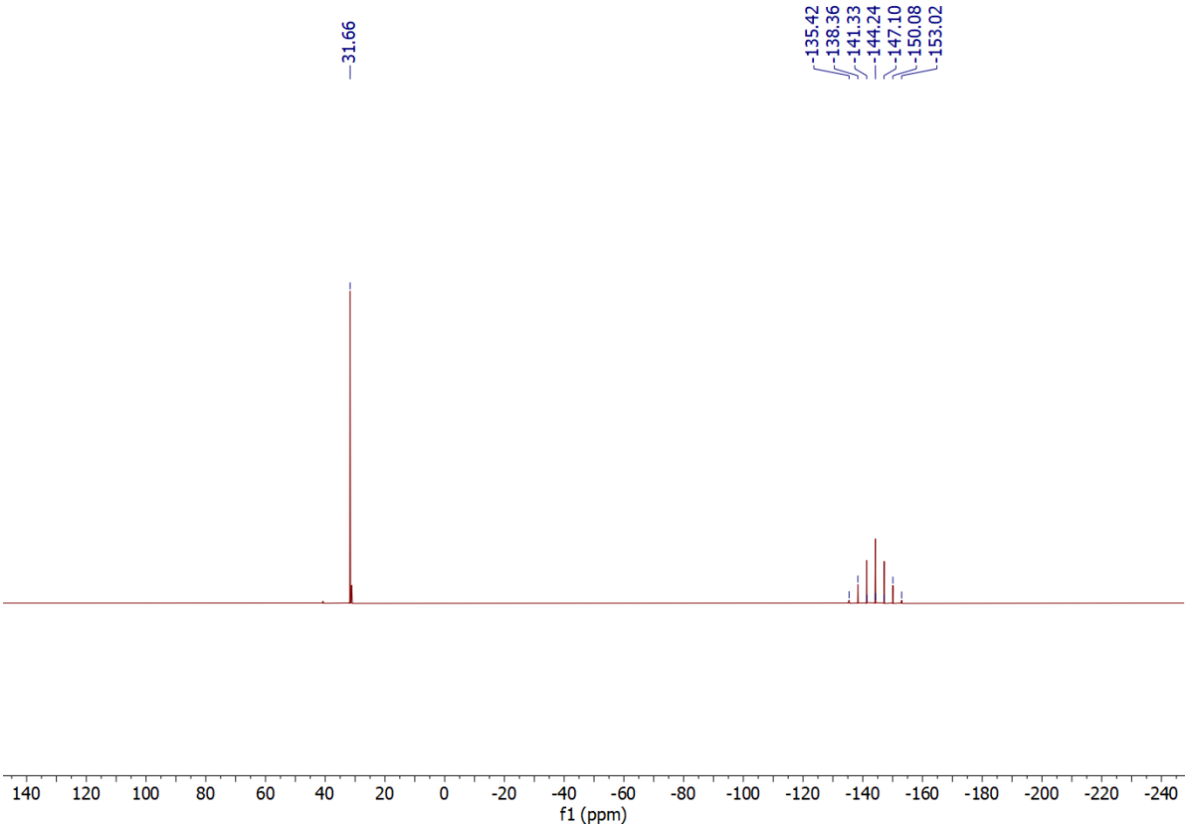

Fig. S2k: $^{31}P\{^{1}H\}$ NMR spectrum (202 MHz, $CDCl_3$) of complex **3**.

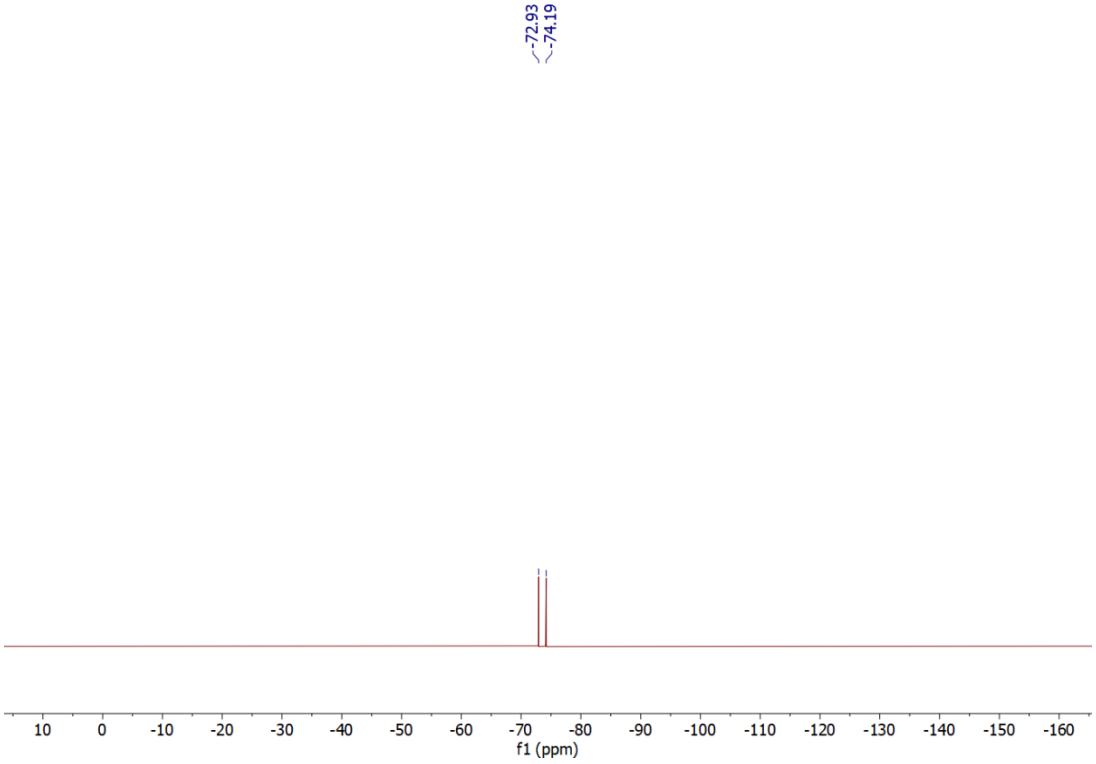

Fig. S2l: $^{19}F\{^{1}H\}$ NMR spectrum (470 MHz, $CDCl_3$) of complex **3**.

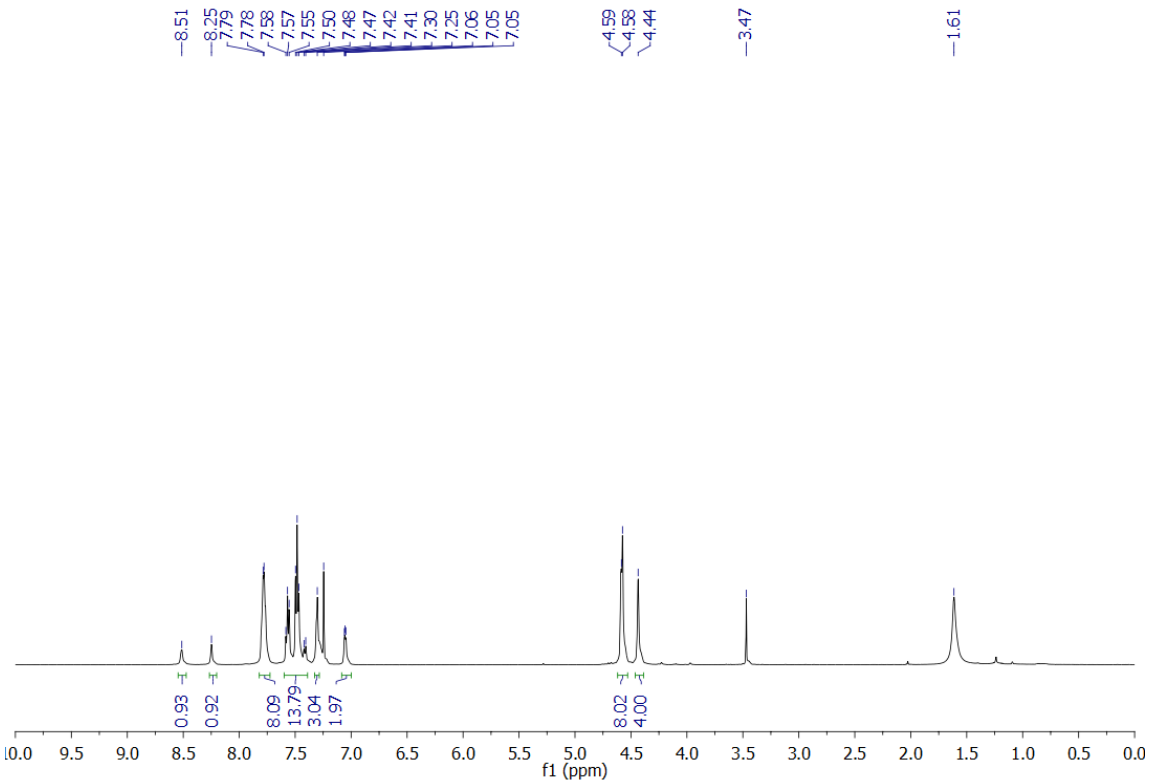

Fig. S2m: ^{1}H NMR spectrum (500 MHz, $CDCl_3$) of complex **4**.

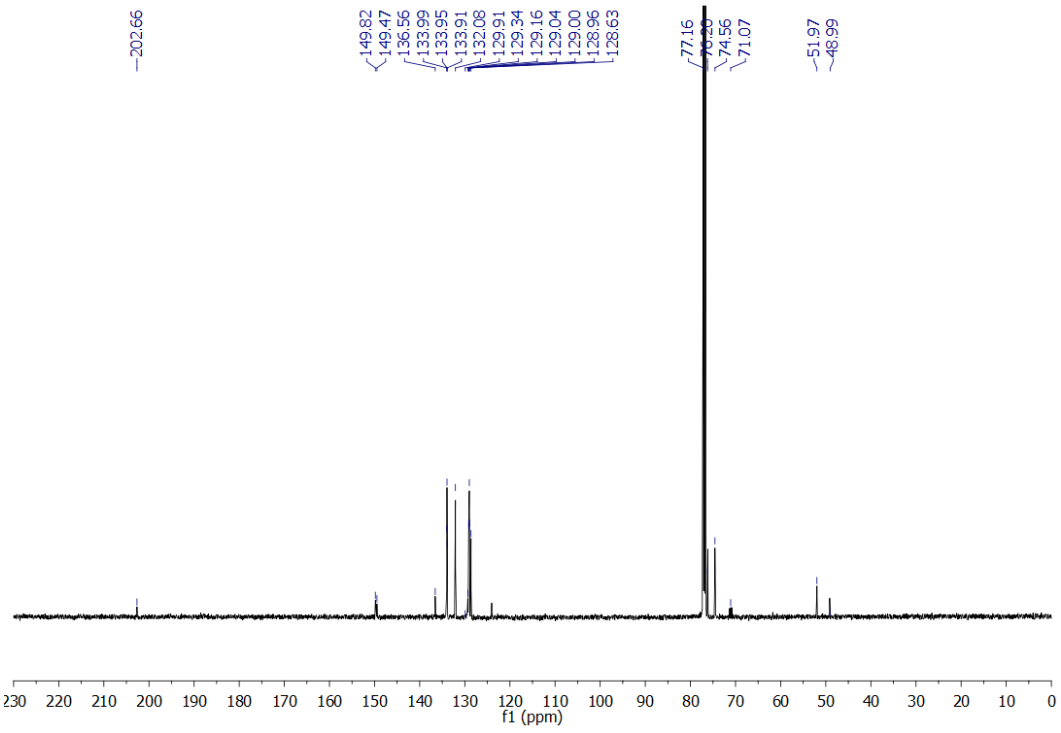

Fig. S2n: $^{13}C\{^{1}H\}$ NMR spectrum (125 MHz, $CDCl_3$) of complex **4**.

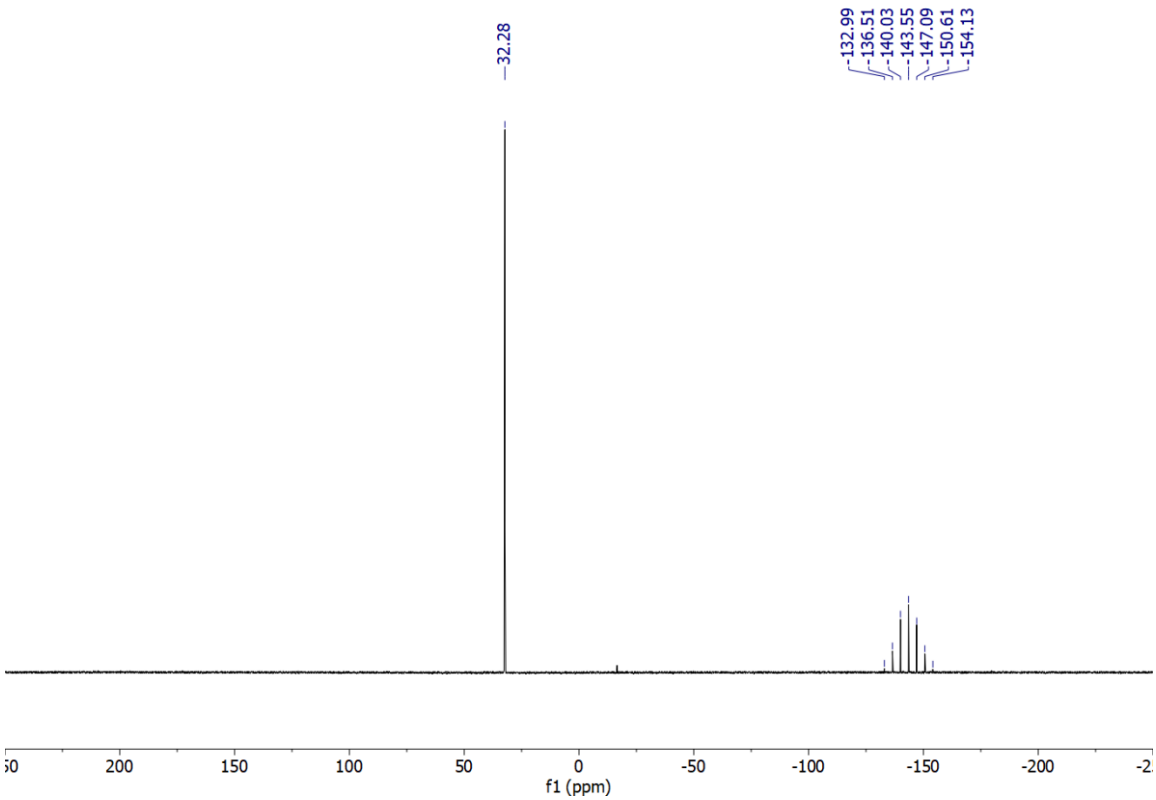

Fig. S2o: $^{31}P\{^{1}H\}$ NMR spectrum (202 MHz, $CDCl_3$) of complex **4**.

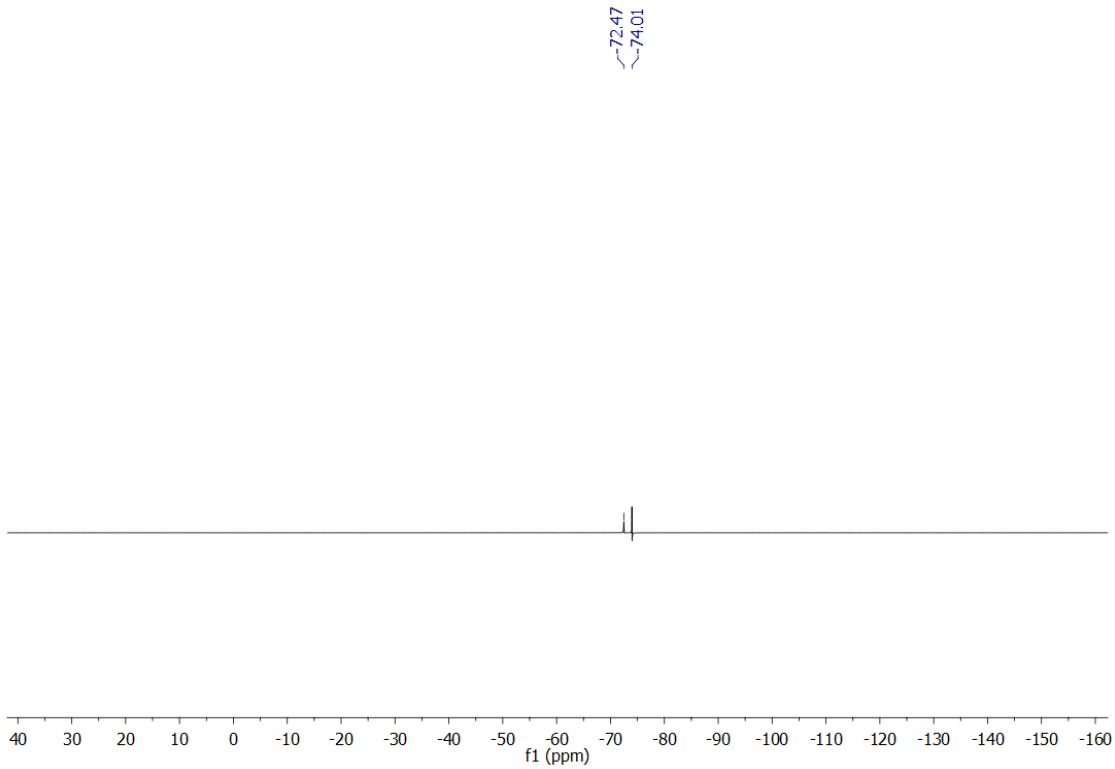

Fig. S2p: $^{19}F\{^{1}H\}$ NMR spectrum (470 MHz, $CDCl_3$) of complex **4**.

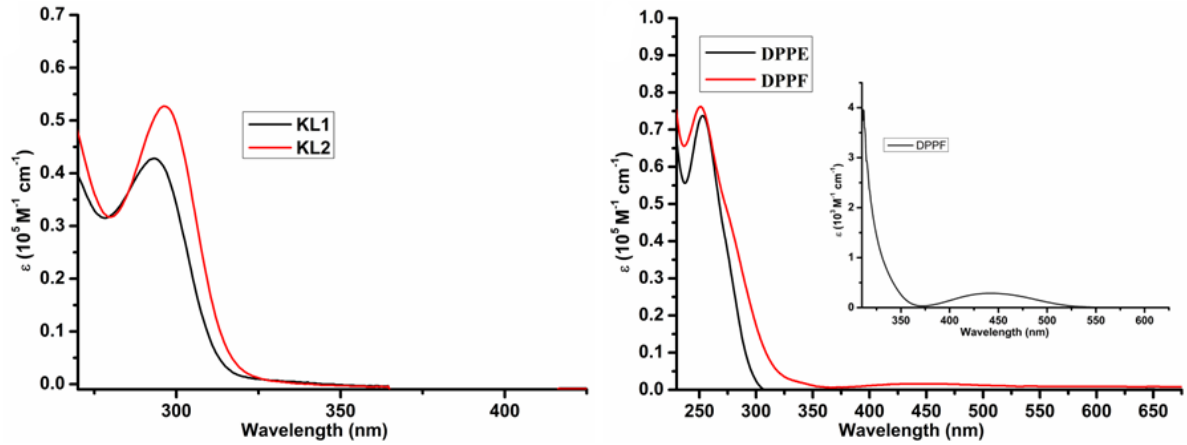

Fig. S3 UV-Vis absorption spectra of dithiocarbamate (**KL1-KL2)** in methanol, and diphosphine **(**dppe, dppf) ligands in dichloromethane solution at 10^{-5} and 10^{-3} molar concentration.

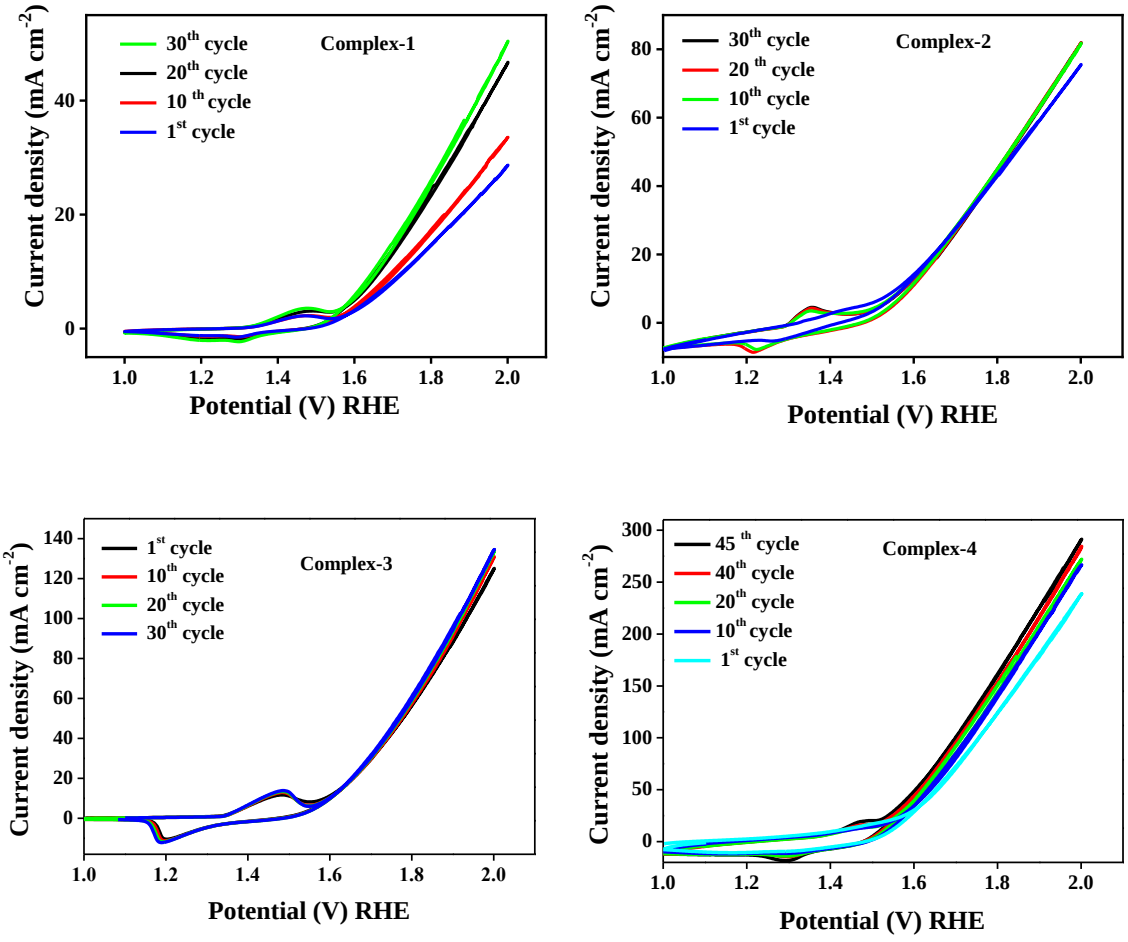

Fig. S4: CV profiles for the electrochemical activation of (a) complex **1**; (b) complex **2**; (c) complex **3**; and (d) complex **4** (scan rate 20 mV s^{-1}, without i*R* correction).

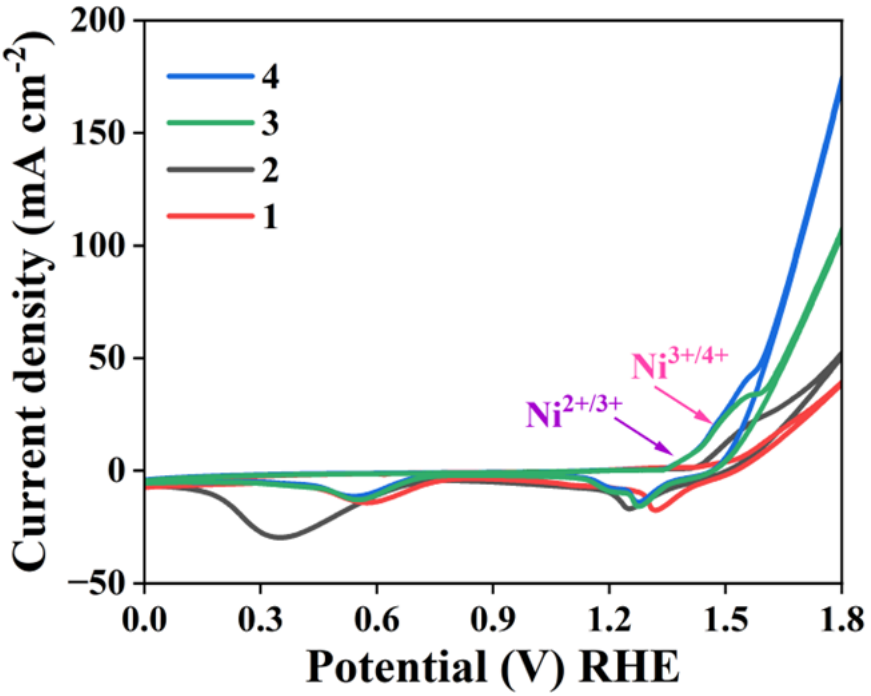

Fig. S5: CV profiles of anodically activated complexes **1- 4@CC**.

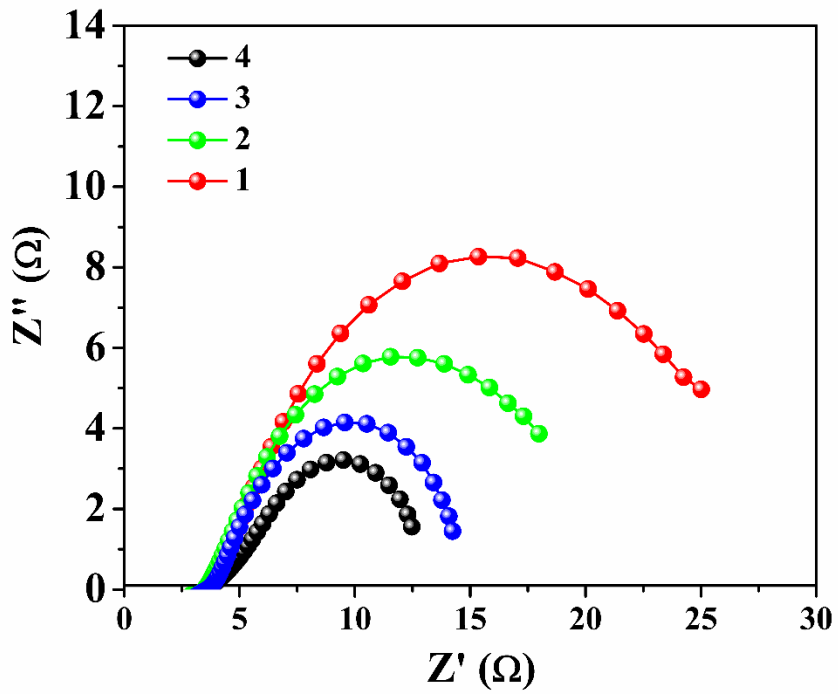

Fig. S6: EIS curves showing the lowest charge transfer resistance for the active catalyst derived from complex **4** compared to active catalysts derived from complexes **1**-**3**.

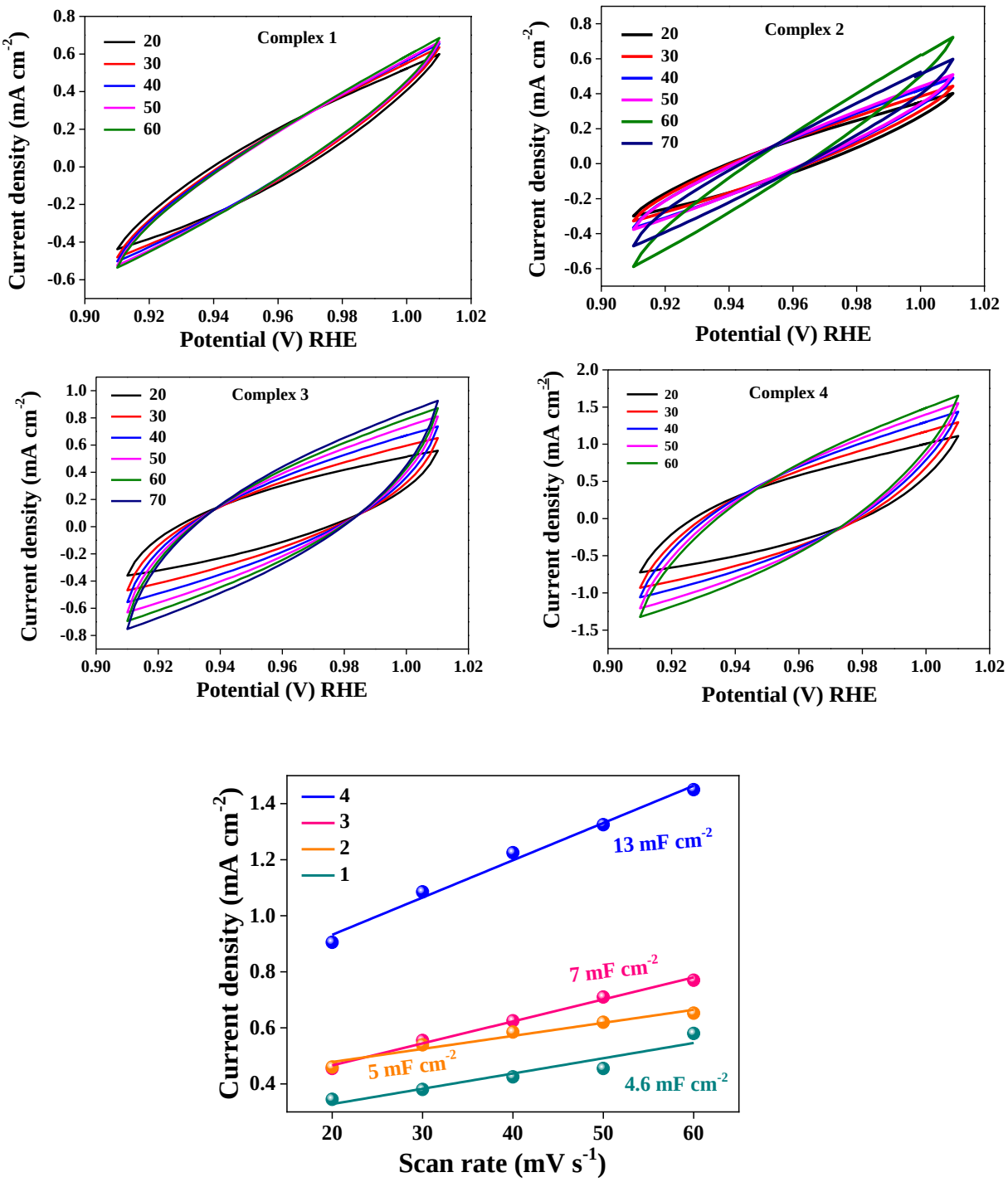

Fig. S7: CV of the activated complexes in the non-faradaic potential region with the variation in the scan rate and the determination of C_{dl} in 1.0 M KOH solution.

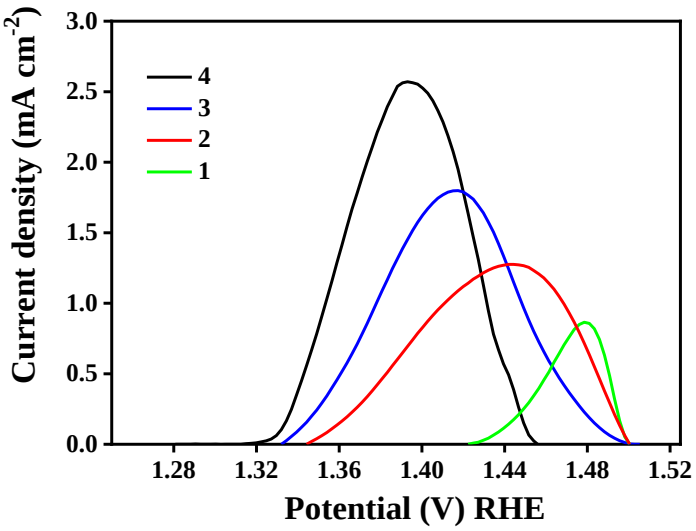

Fig. S8: Redox peak integration for the determination of number of active sites for the active catalyst derived from complexes **1-4**.

Equation S1. **Determination of the number of active sites**

The number of active sites in the catalysts was calculated by the redox peak integration method.

Complex 4:

Calculated area associated with the oxidation peak = 0.181×10^{-3} V A

Hence the associated charge was = 0.181×10^{-3} V A/ 0.005 V s^{-1}

= 36.2×10^{-3} As

= 36.2×10^{-3} C

Now, the number of electron transferred was = 36.2×10^{-3} C/1.602×10^{-19} C

The number of electron calculated above was same as the number of surface active site due to single electron transfer involving Ni^{2+} to Ni^{3+} oxidation process

Hence,

The surface active site of 4 that participated in OER = **22.48×10^{16}**

Complex 3:

Calculated area associated with the oxidation peak = 0.156×10^{-3} V A

Hence the associated charge was = 0.156×10^{-3} V A/ 0.005 V s^{-1}

= 31.2×10^{-3} As

= 31.2×10^{-3} C

Now, the number of electron transferred was = 31.2×10^{-3} C/1.602×10^{-19} C

= 19.47×10^{16}

The number of electron calculated above was same as the number of surface active site due to single electron transfer involving Ni^{2+} to Ni^{3+} oxidation process

Hence,

The surface-active site of 3 that participated in OER =**19.47 × 10^{16}**

Complex 2:

Calculated area associated with the oxidation peak = 0.140 × 10^{-3} V A

Hence the associated charge was = 0.140 × 10^{-3} V A/ 0.005 V s^{-1}

= 28 × 10^{-3} As

= 20 × 10^{-3} C

Now, the number of electron transferred was = 28 × 10^{-3} C/1.602× 10^{-19} C

17.47 × 10^{16}

The number of electron calculated above was same as the number of surface active site due to single electron transfer involving Ni^{2+} to Ni^{3+} oxidation process

Hence,

The surface-active site of 2 that participated in OER = **17.47 × 10^{16}**

Complex 1:

Calculated area associated with the oxidation peak = 0.056 × 10^{-3} V A

Hence the associated charge was = 0.056 × 10^{-3} V A/ 0.005 V s^{-1}

= 11.2 × 10^{-3} As

= 11.2 × 10^{-3} C

Now, the number of electron transferred was = 11.2 × 10^{-3} C/1.602× 10^{-19} C

= **6.99 × 10^{16}**

The number of electron calculated above was the same as the number of the surface-active sites due to single electron transfer involving Ni^{2+} to Ni^{3+} oxidation process

Hence,

The surface-active site of 1 that participated in OER = **6.99 × 10^{16}**

Equation S2. Determination of Turn-Over Frequency (TOF)

The TOF of the complexes can be determined using the equation

TOF = (j × N_A)/ (4 × F × n)

Where, j = current density at 1.48 V vs. RHE

N_A = Avogadro number

F = Faraday constant

n = number of active Ni-sites

For Complex 4:

TOF = (10×10^{-3}) $(6.023 \times 10^{23})/(96485) \times (4) \times (22.48 \times 10^{16})$

TOF = $6.94 \times 10^{-2}\ s^{-1}$

For Complex 3:

TOF = (4.02×10^{-3}) $(6.023 \times 10^{23})/(96485) \times (4) \times (19.47 \times 10^{16})$

TOF = $3.38 \times 10^{-2}\ s^{-1}$

For Complex 2:

TOF = (1.48×10^{-3}) $(6.023 \times 10^{23})/(96485) \times (4) \times (17.47 \times 10^{16})$

TOF = $1.32 \times 10^{-2}\ s^{-1}$

For Complex 1:

TOF = (0.82×10^{-3}) $(6.023 \times 10^{23})/(96485) \times (4) \times (6.99 \times 10^{16})$

TOF = $1.78 \times 10^{-2}\ s^{-1}$

Equation S3: Calculation of exchange current density

The exchange current density of the complexes can be determined using the equation (*J. Energy Chem.*, 2022, **67**, 101-137)

$\boldsymbol{J_0 = RT/nFR_{ct}}$

Where, **R** = gas constant (8.314 J mol^{-1} K^{-1})

T= temperature (298 K)

n = number of electron transfer

F = Faraday's constant (96485 C mol^{-1})

$\boldsymbol{R_{ct}}$ = charge transfer resistance (obtained from EIS)

Active catalysts from	$\boldsymbol{R_{ct}}$ **value (Ω)**	**Exchange current density (A cm^{-2})**
Complex **1**@CC	21.63	2.9×10^{-4}
Complex **2**@CC	14.42	4.4×10^{-4}
Complex **3**@CC	10.92	5.8×10^{-4}
Complex **4**@CC	9.03	7.1×10^{-4}

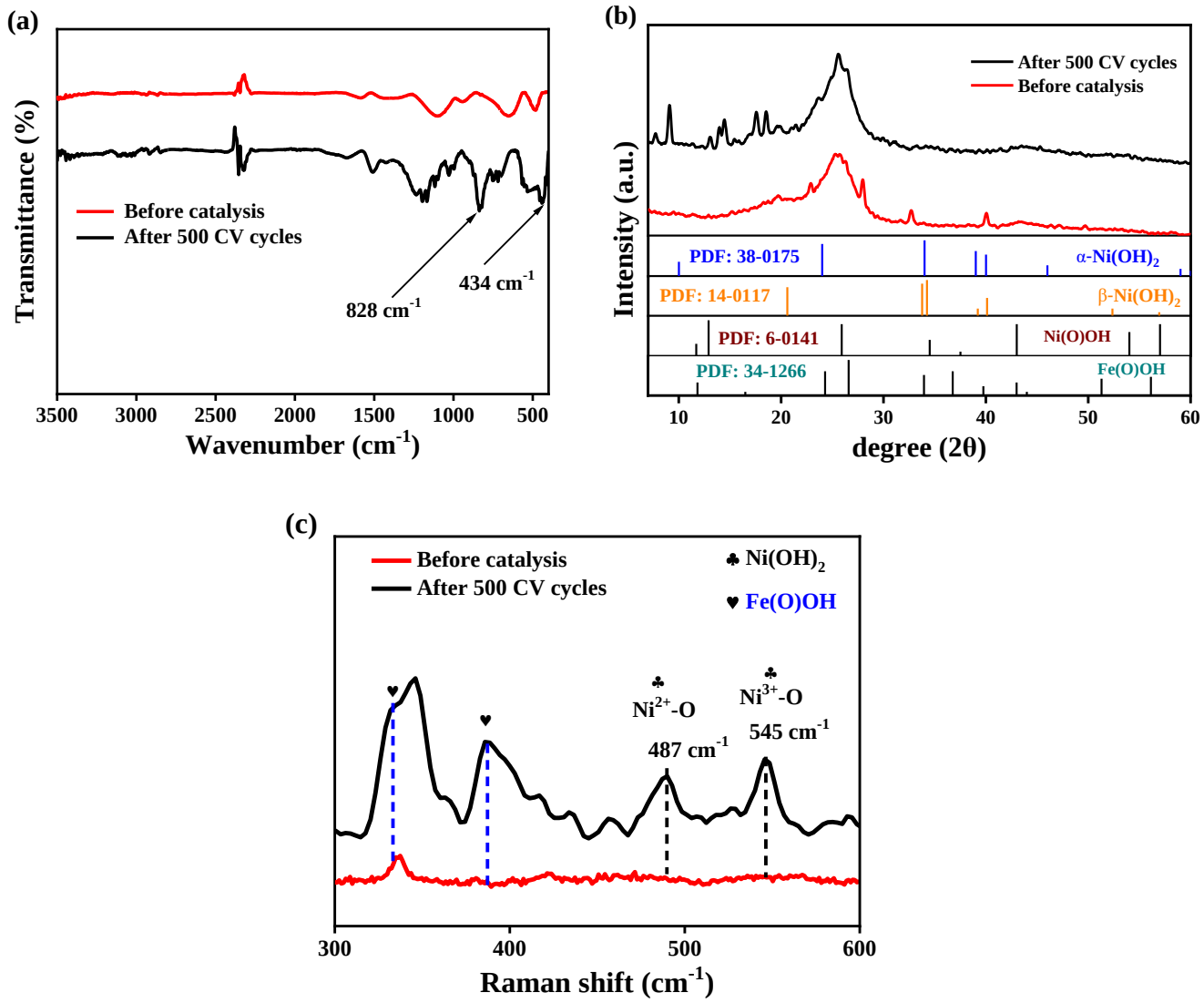

Fig. S9. **(a)** The FT-IR spectrum of active catalyst derived from complex **4@CC** after 500 CV cycles shows new peaks at 828 cm^{-1} and 434 cm^{-1}, which are attributed to the Ni–O bond stretching; **(b)** The powder XRD pattern of active catalyst derived from complex **4@CC** after 500 CV cycles indicates that the molecular structure has disappeared and transformed into $Ni(OH)_2$/Ni(O)OH- β-Fe(O)OH. **(c)** The Raman spectra of complex **4** before and after the 500 CV cycles also demonstrate structural reconstruction. The appearance of two peaks at 487 cm^{-1} and 545 cm^{-1} confirms the formation of $Ni(OH)_2$/Ni(O)OH, while the peaks at 331 cm^{-1} and 385 cm^{-1} demonstrate the β-phase of Fe(O)OH. (*Adv. Energy Mater.*, 2022, **12**, 2103383)

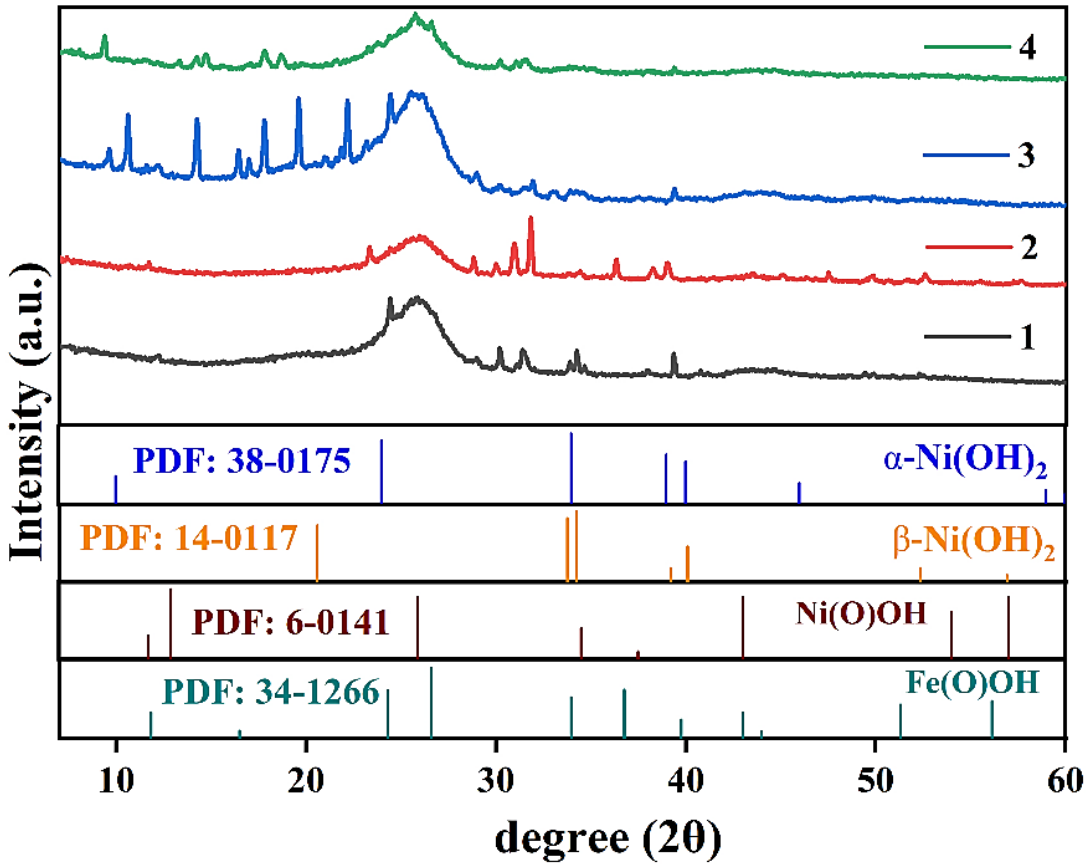

Fig. S10: The powder XRD patterns of active catalysts derived from complexes **1-4@CC** after 100 CV cycles. It was observed that the molecular structures had transformed into $Ni(OH)_2$/Ni(O)OH (JCPDS No. 38-0715 and 6-0141). With complexes **1** and **3**, only $Ni(OH)_2$ peaks were detected, while with complexes **2** and **4**, both $Ni(OH)_2$ and Ni(O)OH peaks were observed. This suggests that complexes **1** and **3** were activated to $Ni(OH)_2$ as active catalyst, whereas complexes **2** and **4** were activated to both $Ni(OH)_2$ and Ni(O)OH as active catalyst. Additionally, the peaks for β-phase of Fe(O)OH (JCPDS No. 34-1266) were also detected in the active catalysts derived from complexes **3** and **4**.

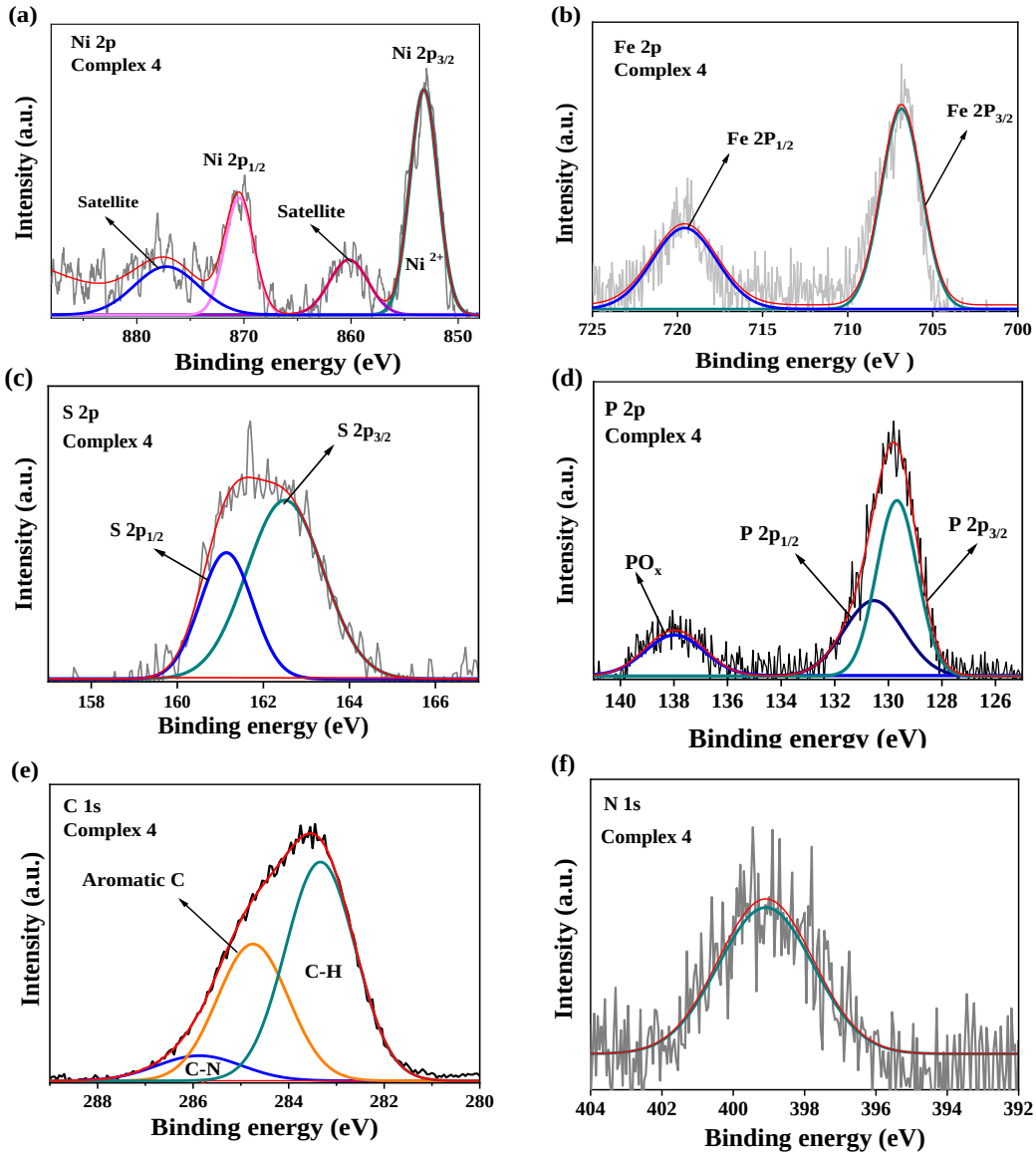

Fig. S11: XPS of synthesized complex **4**. **(a)** Ni 2p XPS showing the peaks at 853.19 eV and 870.53 eV assigned for the Ni $2p_{3/2}$ and Ni $2p_{1/2}$, respectively. The peak at 853.93 eV was attributed to Ni^{2+} species; **(b)** Fe 2p XPS showing the peaks at 706.81 eV and 719.65 eV assigned for the Fe $2p_{3/2}$ and Fe $2p_{1/2}$, respectively; **(c)** S 2p XPS indicating two peaks at 161.13 eV and 162.49 eV attributed to the S $2p_{3/2}$ and S $2p_{1/2}$, respectively; **(d)** P 2p XPS showing three peaks at 136.21 eV, 132.05 eV, and 130.55 eV, the peaks at 130.55 eV, and 132.05 eV were attributed to $2p_{3/2}$ and $2p_{1/2}$ while 136.21 eV corresponds to PO_x species; (*J. Chem. Phys.*,1987, **87**, 5002–5006) ; **(e)** C 1s XPS showing three peaks at 285.94 eV, 284.75 eV and 283.33 eV corresponded to C-N bond, aromatic C and C-H bond respectively; **(f)** N 1s XPS indicated a peak corresponding to the C–N (398.51 eV) bond.

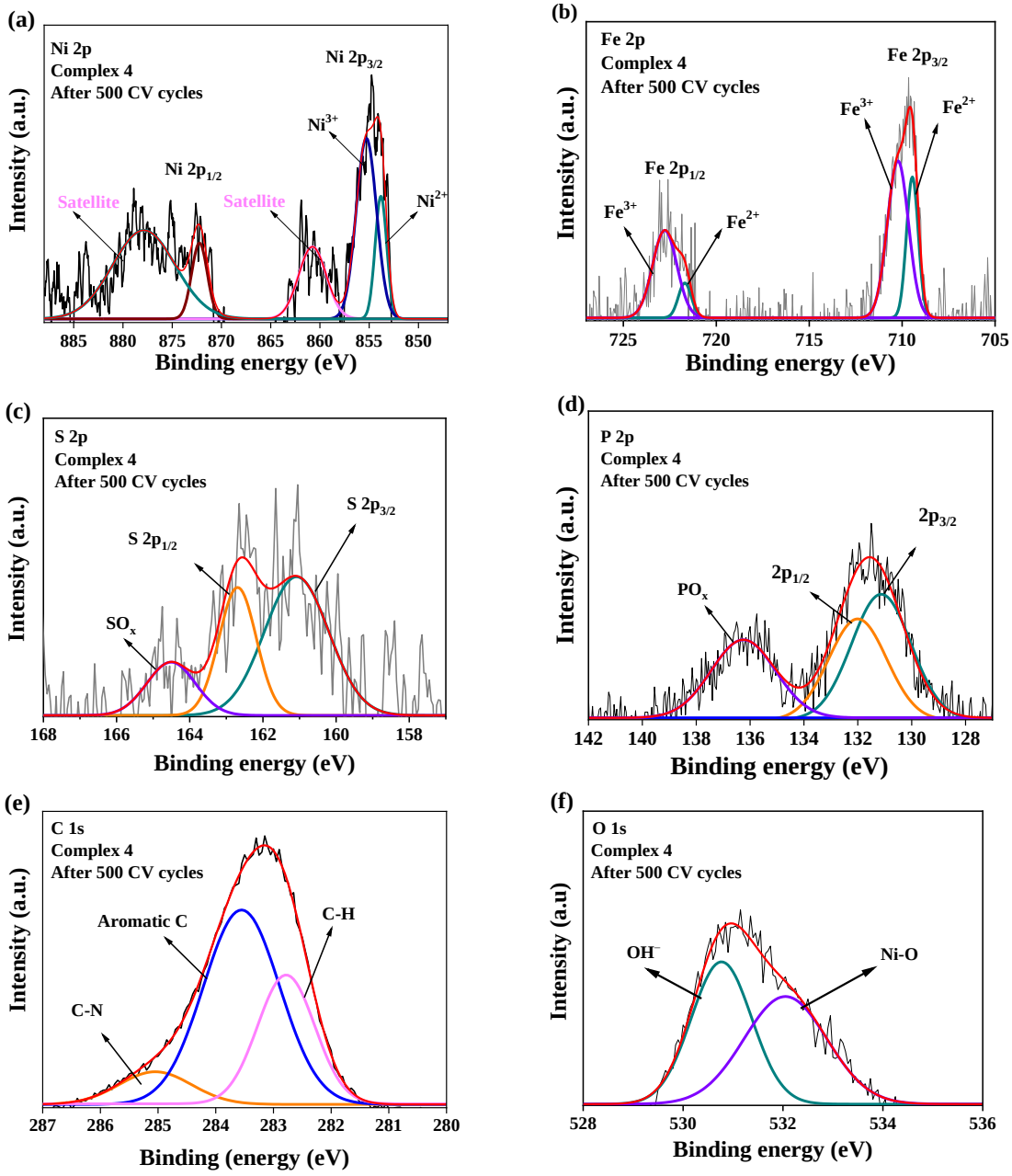

Fig. S12: XPS of active catalyst derived from complex **4** after 500 CV cycles **(a)** Ni 2p XPS showing the peaks at 853.86 eV, and 872 eV assigned for the Ni $2p_{3/2}$ and Ni $2p_{1/2}$, respectively, the peaks at 853.90 eV and 855.19 eV was attributed to the Ni^{2+} and Ni^{3+} species; **(b)** The Fe 2p XPS of complex displays peaks for Fe $2p_{3/2}$ and Fe $2p_{1/2}$, the peaks cantered at 709.31 eV and 721.60 eV are attributed to Fe^{2+}, while peaks at 710.42 eV and 723.18 eV correspond to Fe^{3+} ; **(c)** S 2p XPS indicating three peaks at 161.21 eV, 162.73 eV, and 163.81 eV attributed to the S $2p_{3/2}$, S $2p_{1/2}$, and SO_x species, respectively; **(d)** P 2p XPS showing three peaks at 129.71 eV, 130.81 eV and 136.32 eV, assigned for P $2p_{3/2}$, P $2p_{1/2}$, and PO_x species, respectively; **(e)** C 1s XPS showing three peaks at 285.10 eV, 283.57 eV, and 282.73 eV

corresponding to C-N bond, aromatic C, and C-H bond, respectively; **(f)** O 1s XPS indicating two peaks at 530.75 eV and 532.07 corresponding to OH^- and Ni-O bond.

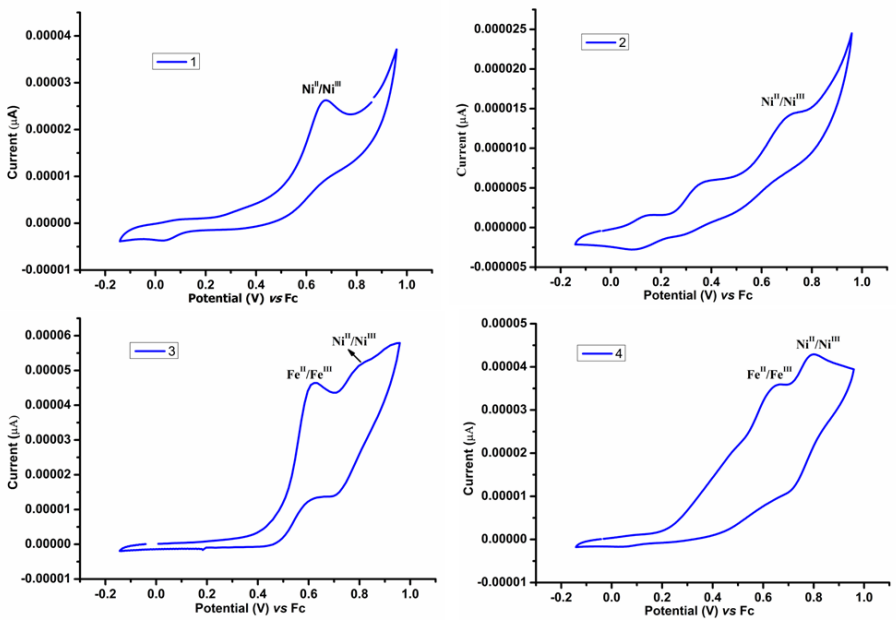

Fig. S13: Cyclic voltammograms (CVs) of complexes **1–4 (**1 mM) in acetonitrile solution containing 0.1 M $TBAPF_6$ supporting electrolyte at a scan rate of 100 mV. The glassy carbon electrode (GCE) with a 2 mm diameter served as the working electrode, platinum wire as the counter electrode, and $Ag/AgNO_3$ as the reference electrode.

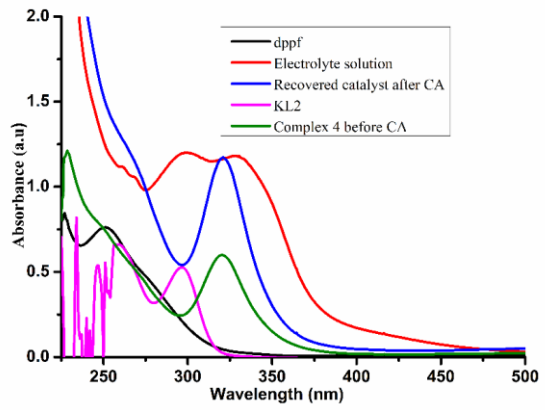

Fig. S14: UV-Vis. spectra of dppf, electrolyte solution, KL2 ligand, complex **4** before and after CA.

Table S1. A literature survey table compares the OER performance of related Ni(II)-based catalysts

Catalyst[a]	Electrolyte	Overpotential (mV)	TOF	Reference
Ni[(TMC)(CH_3CN)](NO_3)$_2$	Phosphate buffer	590 mV @0.5 mA cm^{-2}	-	*Chem. Commun*., 2019, **55**, 6122–6125.
[NiL](PF_6)$_2$	Phosphate buffer	270 mV @0.65 mA cm^{-2}	-	*Catal. Sci. Technol.*, 2019, **9**, 5651–5659.
Ni–Hmfchce	0.1 KOH	490 mV @10 mA cm^{-2}	-	*Polyhedron*, 2019, **174**, 114160.
Ni(II)1,1-dithiolate-phosphine	1.0 M KOH	350 mV @10 mA cm^{-2}	-	*Dalton Trans.*, 2020, **49**, 3592.
Ni-MOG	0.1 M KOH	418 mV @10 mA cm^{-2}	-	*ChemCatChem*, 2023, **15**, e202300694.
$LaNiO_{2.9}F_{0.1}$	1.0 M KOH	320 mV @10 mA cm^{-2}	-	*ACS Catal.*, 2024, **14**, 15096−15107.
N−Co−Mo−GF/ CNT on Ni	0.1 M KOH	330 mV @10 mA cm^{-2}, 350 mV @50 mA cm^{-2}	-	*ACS Catal*., 2020, **10**, 4647−4658.
Ni_5P_4 Films/Ni foil	1.0 M KOH	150 mV @10 mA cm^{-2}	-	*Angew. Chem. Int. Ed.*, 2015, **54**, 12361–12365.
Ni(II) dithiocarbamate	1.0 M KOH	330 mV @10 mA cm^{-2}	5.2×10^{-1} s^{-1}	*Dalton Trans.*, 2023, **52**, 936–946.
α-Ni(OH)$_2$	0.1 M KOH	331 mV @10 mA cm^{-2}	3.61×10^{-2} s^{-1}	*J. Am. Chem. Soc.*, 2014, **136**, 7077−7084
$(bpy)_zNiO_xH_y$ (bpy = 2,2′-bipyridine)	1.0 M NaOH	300 mV @1.0 mA cm^{-2}	1.1 s^{-1}	*ACS Appl. Mater. Interfaces*, 2021, **13**, 48661−48668.
[Ni(S^S)(P^P)]PF_6	1.0 M KOH	250 mV @10 mA cm^{-2}	6.94×10^{-2} s^{-1}	This work